

Institut für Computergraphik und  
Algorithmen

Technische Universität Wien

Karlsplatz 13/186/2

A-1040 Wien

AUSTRIA

Tel: +43 (1) 58801-18601

Fax: +43 (1) 58801-18698

Institute of Computer Graphics and  
Algorithms

Vienna University of Technology

*email:*

[technical-report@cg.tuwien.ac.at](mailto:technical-report@cg.tuwien.ac.at)

*other services:*

<http://www.cg.tuwien.ac.at/>

<ftp://ftp.cg.tuwien.ac.at/>

# TECHNICAL REPORT

## **Inconsistent Shadows for Volume Rendering**

P. Sikachev<sup>1</sup>, P. Rautek<sup>1</sup>, S. Bruckner<sup>1</sup>, and M. E. Gröller<sup>1</sup>

<sup>1</sup>Institute of Computer Graphics and Algorithms, Vienna University of Technology, Vienna, Austria

TR-186-2-11-1

October 2011



# Inconsistent Shadows for Volume Rendering

P. Sikachev<sup>1</sup>, P. Rautek<sup>1</sup>, S. Bruckner<sup>1</sup>, and M. E. Gröller<sup>1</sup>

<sup>1</sup>Institute of Computer Graphics and Algorithms, Vienna University of Technology, Vienna, Austria

October 19, 2011

## Abstract

In volume rendering shadows provide an important visual cue, and enhance depth perception. However, shadowing has its own disadvantages. Shadows do not take into account the importance of features and could potentially result in too dark scenes.

In this paper we propose an approach for inconsistent shadowing, which is designed to overcome these limitations. For the purpose of illustrative rendering, we propose two complementary techniques: 1. shadow caster inconsistency and 2. shadow receiver inconsistency. We demonstrate several advantages of the different approaches, using inconsistent shadowing. We present two approaches, based on shadow transfer function concept, an approach, introducing usage of gradient magnitude information in shadowing, and a method for adaptive shading and shadowing of the surface, depending on the gradient certainty.

Categories and Subject Descriptors (according to ACM CCS): Computer Graphics [I.3.7]: Three-Dimensional Graphics and RealismColor, shading, shadowing, and texture

## 1 Introduction

Shading is an important step of the effective direct volume rendering pipeline [DCH88]. Different shading algorithms (such as Phong shading) are extensively used to provide the user with visual cues about the shape of the depicted object. The surface normal is approximated with the gradient at each sample location.

As a local lighting model, shading fails to provide depth cues, especially, for highly curved regions. To overcome this limitation, shadowing can be used. It helps to emphasize the cavities of the model and can provide a better understanding of the shape of potentially complex objects. Figure 1 shows different combinations of

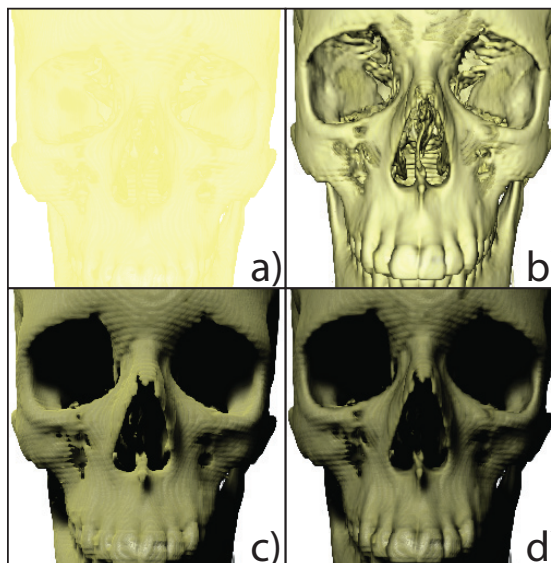


Figure 1: Different rendering techniques for a human skull dataset: a) no shading or shadowing, b) shading only, c) shadowing only, d) shading and shadowing.

shading and shadowing. Notice, how shadows emphasize the spatial relations in the regions of the eyes, jaw, and nose and how shading reveals the detailed structure of the teeth and bones.

The disadvantages of shadowing are: too dark result images, which causes a loss of information, and inflexibility, causing darkening (or even removal) of important features. In order to overcome these limitations, artists sacrifice photorealism for the sake of expressiveness, and use *inconsistent* shadowing.

In this paper we research the properties of inconsistent shadows and their applications for volume rendering. In particular, we propose the classification for such methods and provide examples, which mimic existing illustration techniques.

The paper is organized as follows. In Section 2 we describe related work. In Section 3 we present our inconsistent shadow classification and describe corresponding algorithms. In Section 4 we discuss implementation details. In Section 5 we show results and discuss them. We conclude and propose future research directions in Section 6.

## 2 Related Work

In recent years, a lot of work has been performed in the area of shadow algorithms for volume rendering. Deep shadow maps [LV00] have recently been adopted for interactive volume rendering [HKSB06]. Schott et al. proposed an approach for shadows in slice-based volume rendering [SPH\*09]. It has recently been extended with the possibilities of multi-light rendering and accurate shadow blurring [vPBV10]. A method, working for an arbitrary light source position, was introduced by Ropinski et al. [RDRS10].

Illustrative rendering has become a topic of interest over the last years. The idea of volume illustration was at the first time presented by Ebert and Rheingans [ER00]. The concept of importance-driven rendering was introduced by Viola et al. [VKG04], where several approaches for emphasizing *focus* parts while keeping the *context* were presented. Another context-preserving approach, described by Bruckner et al. [BGKG05], presents a method, inspired by the 'ghosting' technique in traditional illustration. Unlike previously described methods, an approach by Bruckner and Gröller [BG06] changes the geometry of the model in order to show the *context* regions. To bring together different shading schemes, style transfer functions [BG07b] were introduced. Although a lot of illustrative volume-rendering methods have been developed, little attention has been paid to shadows in illustration, which are extensively used in the medical area. Volumetric halos were proposed by Bruckner and Gröller [BG07a], however, they produce a local shading effect, which sometimes may be insufficient.

Recently some work has been performed in the direction of non-photorealistic modification of lighting (i.e., using inconsistent lighting) in order to better depict details. For polygonal rendering, a method, based on the dynamical adjustment of the effective light position for different areas of the surface, was introduced by Rusinkiewicz et al. [RBD06]. After that, a light warping technique (which means changing the range of an environment-map patch, projected on the particular part of the surface) was proposed by Vergne et

al. [VPB\*09] in order to emphasize the details on the object surface. It was further developed and improved in follow-up work [VPB\*10]. In the field of volume rendering, a method, proposed by Díaz et al. [DMV10] is using unsharp masking in mip-mapped volumes in order to enhance the rendering of surface details.

Contour visualization has also recently captured the attention of the community. Cséfalvi et al. [CMH\*01] proposed a fast visualization technique for object contours of volumetric data, which uses magnitude of local gradient information. DeCarlo et al. [DFRS03] described two methods for contour depiction, based on the radial curvature estimation. These methods proved to be more effective than traditional contours. Kolomenkin et al. [KST08] suggested to use the loci of the "strongest" inflections on the surface. They achieve more stable results than previous methods, such as in the work of Judd et al. [JDA07].

Thus, quite a lot of work has been done in the field of shadowing for volume rendering, inconsistent lighting, and illustrative methods. None of these methods employ inconsistent shadowing, which is extensively used in illustration. In this paper, we propose a pipeline for inconsistent shadowing and demonstrate it with various examples.

## 3 Inconsistent Shadowing

Considering a shadow, three entities are involved. First, a light ray is cast by a particular *light source*. When the ray hits a surface - we call this surface *shadow caster*. If we follow the ray up to the next intersection with some other surface - this surface is called *shadow receiver*, as it is in shadow because of the shadow caster.

In the case of volume rendering the scenario is more complex. Instead of surfaces we deal with semi-transparent volume samples. Each of the samples is a shadow receiver, as well as a shadow caster, shown in Figure 2. Conceptually, this does not affect conceptually our approach.

In our framework, we consider two stages: a ray hits a shadow caster and a ray hits a shadow receiver. We classify shadowing inconsistency-techniques depending on the stage where they occur. For each stage, one or several techniques might be applied, and then the effects on different stages can be merged, as described in Section 6. We will discuss the techniques available in the following subsections. Throughout the paper we will terminology (i. e., *transfer function*), introduced by Hadwiger et al. [HKRs\*06].

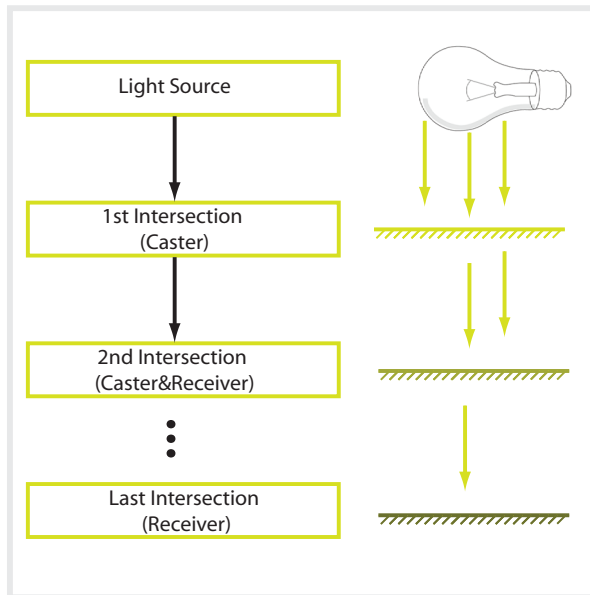


Figure 2: Shadow casters and shadow receivers. Notice that the light energy decreases the more the ray travels through the volume.

### 3.1 Shadow Caster Inconsistency

Normally, the more opaque an object is, the more opaque the shadow is it casts. However, that is not always the case in illustrations. Figure 3(a) shows an example of such an inconsistency. Notice, that bones are self-shadowed, but are not shadowed by the blood vessels. We call this method a *shadow caster inconsistency*.

In our pipeline this effect is modelled with a shadow, selectively cast by the bones only (as they could be easily segmented even with a regular 1D transfer function). To provide a user with a flexible instrument for specifying which structures should cast shadows, we use a so-called *shadow transfer function*, with a range of  $[0, 1]$ . A value of 0 corresponds to the structures which do not cast shadows, while a value of 1 corresponds to structures which cast shadows normally. As bones and vessels in this dataset do not share the same density, no manual segmentation is needed, but a 1D shadow transfer function (explained in more detail in Section 4.1) is used.

Figures 3(b, c) show the difference of conventional visualization and the proposed approach. Notice that the blood vessel in the illustration as well as in the proposed approach 3(c), do not cast shadows on the bones, contrary to the conventional approach 3(b). Furthermore, with our inconsistent shadowing, samples, classi-

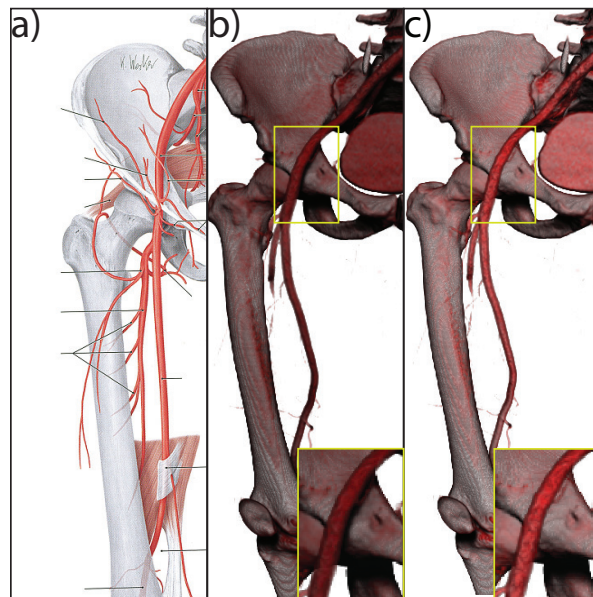


Figure 3: Fragment of a human bone and vessels: a) medical illustration (image courtesy of Georg Thieme Verlag & Wilkins, copyright ©2005), b) volume rendering with conventional shadowing, c) volume rendering with shadow caster inconsistency. As can be observed from the close-ups, applying shadow caster inconsistency allows not to have a shadow, cast by the vessels, on the bones.

fied as blood vessels, are not self-shadowed, preventing the overall darkening of the picture, while preserving bone self-shadowing, as opposed to the regular shadowing.

### 3.2 Shadow Receiver Inconsistency

Though it is important, which object casts a shadow, it is even more important, which object receives a shadow. As mentioned above, some salient features may become less visible on a shadowed object, which should be avoided. Below we present two techniques which mimic existing methods, used in illustrations. Besides, we present a technique which shares the same idea of modifying the shadow on the receiver, but is used for lighting enhancement.

#### 3.2.1 Shadow Receiver Transfer Function

Salient features that are present in the volume are usually critical to understand an object's shape. However, these salient features may be (completely or partially)

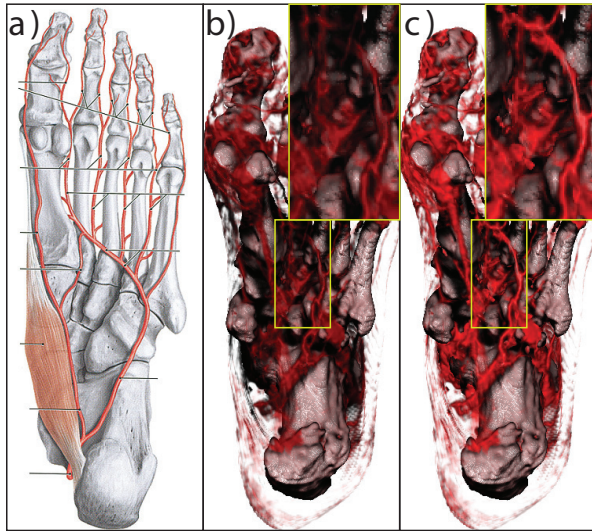


Figure 4: A human foot: a) medical illustration (image courtesy of Georg Thieme Verlag & Wilkins, copyright ©2005), b) volume rendering with conventional shadowing, c) volume rendering with shadow receiver inconsistency. Notice, that using shadow receiver inconsistency allows to distinguish the blood vessels, running through the shadow, much better, than while using the conventional shadowing.

lost in a shadow. In order to overcome this, illustrators use inconsistent shadowing: they put less shadow on the important regions. This approach is illustrated in Figure 4(a). Notice, that the bones are both shadowed by the blood vessels and self-shadowed. However, the blood vessels are neither shadowed nor self-shadowed (because they are important in this case).

We introduce a shadow transfer function, which gives a versatile control over the darkness of the shadow at the shadow receiver. This function has a range of  $[0, 1]$ , where 0 corresponds to the original level of shadow and 1 corresponds to no shadow at all at the receiver.

Figures 4(b) and 4(c) show the results of conventional shadow mapping and applying shadow receiver transfer function respectively. A lot of thin blood vessels, as well as parts of large vessels become better visible with the proposed approach.

### 3.2.2 Contour Preserving Shadowing

In the previous section, a method for preserving the visibility of salient features, has been presented. However, this approach is not universal. One may want to preserve the visibility contours visible while they are in shadow.

Obviously, the previous approach could not be used as it uniformly reduce the shadow on the entire surface, not only on the contours. Illustrators usually pick the contours of the object by leaving them without shadows, as shown in Figure 5(a). Notice how the contours of the eyeholes are highlighted, as well as the contours of the nose and cheeks.

In order to achieve this effect, we introduce a special real-time method which estimates whether a sample corresponds to a contour. This approach is described in more detail in Section 4.3. Samples, lying on the contours are less shadowed or not shadowed at all. This effect is shown in Figure 5(c). It exposes more inner details in eyes and nose areas, and also shows more surface details in the shadowed areas, as compared to the conventional approach, shown in Figure 5(b).

### 3.2.3 Gradient Magnitude-Dependant Shadowing

Shading usually provides a comprehensive information about the shape of a surface. In volume rendering the gradient is used as a normal vector in lighting calculations. The gradient vector can be accurately estimated, volume rendering with a local lighting model produces good results. However, for other parts, e.g., muscle tissue from Figure 6, the gradient direction is not well defined. In this case, straightforward lighting can produce artifacts, which result in noise on the surface not corresponding to reality, as can be observed in Figure 6(a) on the leg muscles.

In order to overcome this, we propose an adaptive method of shading and shadowing. When the gradient is well-defined, shading is applied normally. In case of a poor gradient quality, shadowing is used instead. Unlike just using shadowing, this approach allows to benefit from the advantages of shading and at the same time avoids extensive darkening of the image. We utilize an assumption, that the better a gradient is defined, the higher gradient magnitude it has.

Figure 6 presents a comparison between the approach described in this Section and other techniques. It can be observed, that the method in Figure 6(a) produces strong artifacts in the muscle tissue due to an uncertain gradient estimation. The method shown in Figure 6(b) fails to represent the shape of the muscles. The method in Figure 6(c) darkens the resulting image, hiding important details (see the close-ups in the top left corners). Finally, the method described in this Section (Figure 6(d)) is free from these drawbacks.

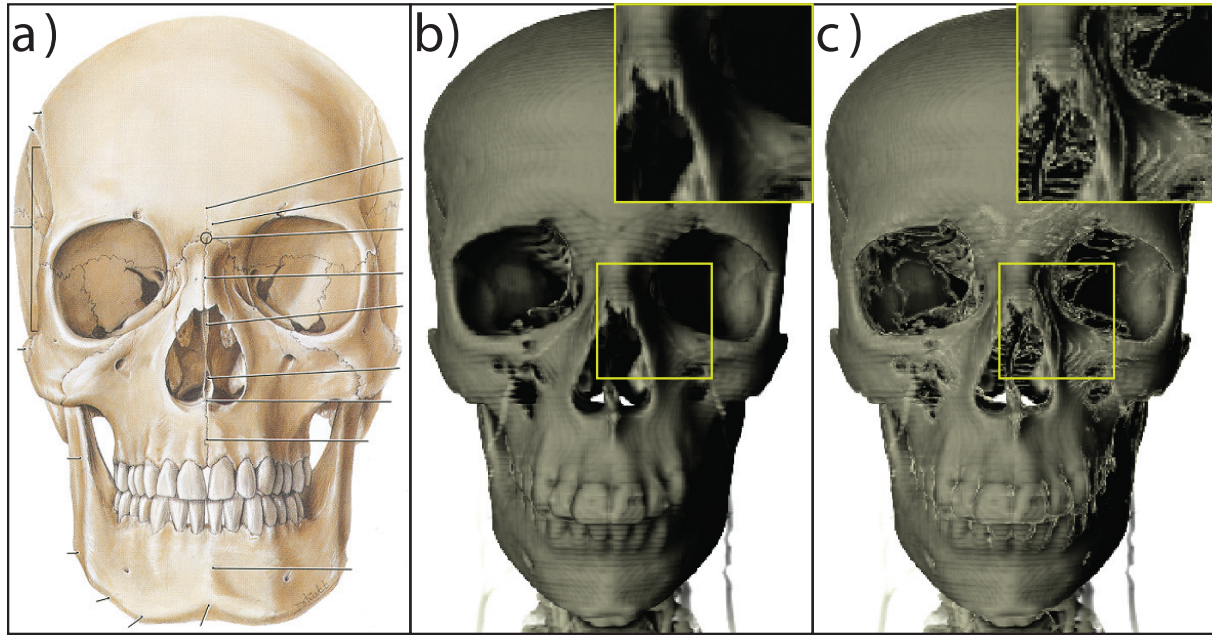


Figure 5: A human skull: a) medical illustration (image courtesy of Lippincott Williams & Wilkins, copyright ©2005), b) volume rendering with conventional shadowing, c) volume rendering with contour-preserving shadowing.

## 4 Implementation

We build our implementation on top of the methods proposed by Šoltészová et al. [vPBV10]. All methods involve mostly shader-code changes and do not invoke a significant computational overhead. Our implementation is not dependant on the actual implementation of the shadow algorithm, therefore it could be easily transferred to other frameworks as well.

### 4.1 1D Shadow Transfer Function

For the shadow caster inconsistency and shadow receiver transfer function the implementation is quite similar. An additional transfer function is introduced, which outputs a scalar value in the range  $[0, 1]$ . So far we experimented only with 1D-transfer functions, but our approach does not impose any limitations on the transfer function.

Equation 1 shows the formula, used for the implementation of the shadow receiver transfer function. Here  $v$  stands for the current sample to be shadowed,  $TF_{col}$  stands for the transfer function color value, obtained at the sample  $v$ ,  $TF_{op}$  stands for the transfer function opacity value, obtained at the same sample,  $C_{shadowed}$  stands for the color after shadowing,  $TF_{sh}$  stands for

a 1D shadow transfer function value,  $O_{acc}$  stands for the opacity value, accumulated so far,  $O_{new}$  stands for the opacity, which will be used for the shading of the next sample,  $TF_{col}$  stands for the transfer function color value of the current sample. The text in bold shows the part of the code, added to the conventional shadow implementation, to implement the proposed approach. It invokes one texture fetch and few arithmetic operations per sample, so it does not significantly affect the performance. This equation assumes the rendering algorithm, which utilizes a front-to-back compositing.

$$C_{shadowed}(v) = (1 - O_{acc} \cdot [\mathbf{1} - \mathbf{TF}_{sh}(v)]) \cdot TF_{col}(v) \quad (1)$$

$$O_{new} = (1 - O_{acc}) \cdot TF_{op}(v)$$

For the shadow caster, a similar algorithm is used. The only difference is that the accumulated opacity value is multiplied by the shadow transfer function value, not the sample color itself. Equation 2 shows further details.

$$C_{shadowed}(v) = (1 - O_{acc}) \cdot TF_{col}(v) \quad (2)$$

$$O_{new} = (1 - O_{acc}) \cdot TF_{op}(v) \cdot \mathbf{TF}_{sh}$$

Figure 7 shows a regular transfer function and the corresponding shadow transfer functions, used to acquire the

results shown in Figure 10. Its domain corresponds to the domain of the regular transfer function, which makes changing the parameters intuitive and straightforward.

## 4.2 Gradient Magnitude-Dependant Shadowing

For gradient magnitude-dependant shadowing we change both, the shading and the shadowing model. For the shading model, we interpolate between Phong shading and no shading, depending on the gradient magnitude, which was proposed by Bruckner and Gröller [BG09]. Equation 3 shows the novel approach:  $C_{unshaded}$  stands for the color with no shading,  $C_{Phong}$  stands for the color with the Phong shading,  $\nabla v$  stands for the gradient vector at the sample  $v$ ,  $|\nabla v|$  stands for the gradient magnitude at the same position,  $g_l$  and  $g_h$  are predefined thresholds for gradient magnitude, and  $smoothstep(x, y, z)$  smoothly transitions from zero to one as  $z$  varies between  $x$  and  $y$ .

$$\begin{aligned} C(v) &= (1 - \lambda)C_{unshaded}(v) + \lambda C_{Phong}(v) \\ \lambda &= smoothstep(g_l, g_h, 1 - (1 - |\nabla v|)^{TF_{op}(v)}) \end{aligned} \quad (3)$$

This interpolation allows us to use the Phong shading for samples with well-defined gradient values (i. e., with high magnitude) and avoid using it for the samples with poorly-defined gradient (in order to avoid shading artifacts due to noisy gradient estimation). However, in this case the structure of these regions is badly conveyed. To overcome this, we use shadowing instead. Equation 4 shows our adaptive approach:

$$C_{shadowed}(v) = (1 - O_{acc} \cdot e^{-\sigma \cdot |\nabla v|}) \cdot TF_{col}(v) \quad (4)$$

$\sigma$  is a predefined constant that controls a degree of gradient magnitude affection on shadowing.  $e^{-\sigma \cdot |\nabla v|}$  is the value added as compared with the conventional shadowing. As the gradient is also used for Phong shading, our implementation does not introduce additional overhead.

## 4.3 Contour-Preserving Shadowing

In order to preserve contours in the shadow, we use a contour-detecting technique, based on [BG07b] which proposes a view-dependent approximation of curvature estimation, presented by Kindlmann et al. [KWTM03]. Equation 5 shows the set of equations, which define whether a sample is shadowed or not:

$$\begin{aligned} \kappa &= \min\left(\frac{1}{\tau}, \frac{|\nabla v - \nabla v_{prev}|}{|v - v_{prev}|}\right) \\ T &= \sqrt{\tau\kappa(2 - \tau\kappa)} \\ \forall samples v : |\nabla v \cdot \vec{r}| &< T \wedge |\nabla v| > \eta \\ &\Rightarrow do\ not\ shadow\ v \end{aligned} \quad (5)$$

$\tau$  stands for the constant, defining contour thickness,  $v_{prev}$  stands for the previous sample on the same ray,  $|v - v_{prev}|$  stands for the distance between these two samples,  $\vec{r}$  stands for the viewing direction, and  $\eta$  stands for the minimal gradient magnitude threshold. The  $|\nabla v| > \eta$  term is used in order to reduce noise, linked with the poorly-defined gradient.

## 5 Results and Discussion

We tested the proposed methods on various datasets. In a number of cases, it produced better visual cues, than traditional techniques. In this section we additionally compare inconsistent shadowing with traditional shading and shadowing techniques, such as:

- no shading
- Phong shading
- regular shadowing
- reduced shadowing (making shadows less dark, than they should be)

In Figure 8 a comparison for the human head dataset is presented.

We use contour-preserving shadowing, for rendering of translucent objects, as contours provide a great deal of shape perception [Tod04]. As can be observed from Figure 9, contour-preserving shadowing 9(d) reveals more inner details than regular and reduced shadowing methods 9(b, c), and show much more of the object's structure, than an approach without shadowing 9(a).

For the 1D transfer function, one of the possible extensions is to combine effects, which take place on the different stages of the shadowing pipeline: at the shadow

receiver and at the shadow caster. The result of this combination is shown in Equation 6.

$$\begin{aligned} C_{shadowed}(v) &= (1 - O_{acc} \cdot [\mathbf{1} - \mathbf{TF}_{sh}(\mathbf{v})]) \cdot TF_{col}(v) \\ O_{new} &= (1 - O_{acc}) \cdot TF_{op}(v) \cdot \mathbf{TF}_{sh} \end{aligned} \quad (6)$$

Figure 10 introduces a comparison between this technique (Figure 10(f)) and other methods. Compared to Figures 10(a, b), the proposed approach provides more visual cues, especially in the lung area. However, unlike Figures 10(c, d, e), it does not introduce too much of the shadow in certain regions, making the vessels, and other structures easily perceivable.

## 6 Conclusion and Future Work

In this paper we presented a concept of inconsistent shadowing pipeline and demonstrated it on several samples, mimicing existing illustration effects. Our pipeline consists of two stages: shadow caster effects and shadow receiver effects. We illustrated shadow caster stage with one effect, and shadow receiver stage - with three effects. A thorough description of the implementation of all the effects was given and results were discussed.

For future research, we have several directions to develop our work. First, a user evaluation will be interesting in order to receive feedback on which effects are useful. Then, more effects should be studied, especially for the shadow caster stage. Another interesting direction is exploring higher dimensional transfer functions, applied to shadows. Also, we made experiments with rendering volumetric shadows to 3D textures. We believe that interesting effects may be achieved by transforming the shadow volume. Finally, we want to apply our shadowing algorithms to uncertainty datasets. We see possibilities to visualize uncertainty using inconsistent shadowing techniques, as much attention is nowadays paid to uncertainty visualization [DPL\*10].

## References

[BG06] BRUCKNER S., GRÖLLER M. E.: Exploded views for volume data. *IEEE Transactions on Visualization and Computer Graphics* (2006), pp. 1077–1084.

[BG07a] BRUCKNER S., GRÖLLER M. E.: Enhancing depth-perception with flexible volumetric halos. *IEEE Transactions on Visualization and Computer Graphics* (2007), pp. 1344–1351.

[BG07b] BRUCKNER S., GRÖLLER M. E.: Style transfer functions for illustrative volume rendering. *Computer Graphics Forum* (2007), pp. 715–724.

[BG09] BRUCKNER S., GRÖLLER M. E.: Instant volume visualization using maximum intensity difference accumulation. *Computer Graphics Forum* (2009), pp. 775–782.

[BGKG05] BRUCKNER S., GRIMM S., KANITSAR A., GRÖLLER M. E.: Illustrative context-preserving volume rendering. In *Proceedings of EuroVis* (2005), pp. 69–76.

[CMH\*01] CSÉBFALVI B., MROZ L., HAUSER H., KÖNIG A., GRÖLLER E.: Fast visualization of object contours by non-photorealistic volume rendering. *Computer Graphics Forum* (2001).

[DCH88] DREBIN R. A., CARPENTER L., HANRAHAN P.: Volume rendering. *SIGGRAPH Computer Graphics* (1988), pp. 65–74.

[DFRS03] DECARLO D., FINKELSTEIN A., RUSINKIEWICZ S., SANTELLA A.: Suggestive contours for conveying shape. *ACM Transactions in Graphics* (2003), pp. 848–855.

[DMV10] DÍAZ J., MARCO J., VÁZQUEZ P.-P.: Cost-effective feature enhancement for volume datasets. In *Proceedings of Vision, Modeling and Visualization* (2010).

[DPL\*10] DIEPENBROCK S., PRASSNI J.-S., LINDEMANN F., BOTHE H.-W., ROPINSKI T.: Pre-operative planning of brain tumor resections. *IEEE Visualization Contest 2010 - Winning Entry*, 2010.

[ER00] EBERT D., RHEINGANS P.: Volume illustration: non-photorealistic rendering of volume models. In *Proceedings of the IEEE Visualization* (2000), pp. 195–202.

[HKRs\*06] HADWIGER M., KNISS J. M., REZK-SALAMA C., WEISKOPF D., ENGEL K.:

- Real-Time Volume Graphics*. A. K. Peters, Ltd., 2006.
- [HKSB06] HADWIGER M., KRATZ A., SIGG C., BÜHLER K.: GPU-accelerated deep shadow maps for direct volume rendering. In *Proceedings of the 21st ACM SIGGRAPH/EUROGRAPHICS symposium on Graphics hardware* (2006), pp. 49–52.
- [JDA07] JUDD T., DURAND F., ADELSON E.: Apparent ridges for line drawing. *ACM Transactions on Graphics* (2007).
- [KST08] KOLOMENKIN M., SHIMSHONI I., TAL A.: Demarcating curves for shape illustration. *ACM Transactions in Graphics* (2008), pp. 157:1–157:9.
- [KWTM03] KINDLMANN G., WHITAKER R., TADIZEN T., MOLLER T.: Curvature-based transfer functions for direct volume rendering: Methods and applications. In *Proceedings of the IEEE Visualization* (2003), pp. 513–520.
- [LV00] LOKOVIC T., VEACH E.: Deep shadow maps. In *Proceedings of the 27th annual conference on Computer graphics and interactive techniques* (2000), SIGGRAPH, pp. 385–392.
- [RBD06] RUSINKIEWICZ S., BURNS M., DECARLO D.: Exaggerated shading for depicting shape and detail. *ACM Transactions on Graphics* (2006), pp. 1199–1205.
- [RDRS10] ROPINSKI T., DÖRING C., REZK-SALAMA C.: Interactive volumetric lighting simulating scattering and shadowing. In *IEEE Pacific Visualization Symposium* (2010), pp. 169–176.
- [SPH\*09] SCHOTT M., PEGORARO V., HANSEN C., BOULANGER K., BOUATOUCH K.: A directional occlusion shading model for interactive direct volume rendering. In *Computer Graphics Forum (Proceedings of Eurographics/IEEE VGTC Symposium on Visualization)* (2009), pp. 855–862.
- [Tod04] TODD J. T.: The visual perception of 3D shape. In *Trends in Cognitive Science* (2004), pp. 115–121.
- [VKG04] VIOLA I., KANITSAR A., GRÖLLER M. E.: Importance-driven volume rendering. In *Proceedings of IEEE Visualization* (2004), pp. 139–145.
- [VPB\*09] VERGNE R., PACANOWSKI R., BARLA P., GRANIER X., SCHLICK C.: Light warping for enhanced surface depiction. *ACM Transactions on Graphics* (2009), pp. 25:1–25:8.
- [VPB\*10] VERGNE R., PACANOWSKI R., BARLA P., GRANIER X., SCHLICK C.: Radiance scaling for versatile surface enhancement. In *Proceedings of the ACM SIGGRAPH symposium on Interactive 3D Graphics and Games* (2010), pp. 143–150.
- [vPBV10] ŠOLTÉSZOVÁ V., PATEL D., BRUCKNER S., VIOLA I.: A multidirectional occlusion shading model for direct volume rendering. *Computer Graphics Forum* (2010), pp. 883–891.

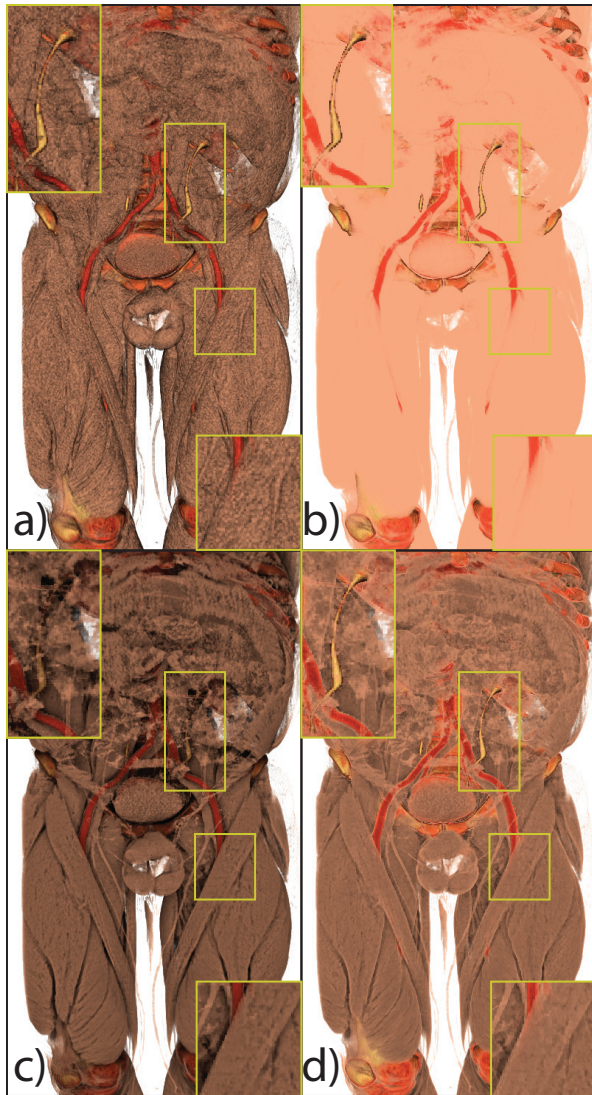


Figure 6: Human body dataset: a) regular shading, b) gradient magnitude-dependant shading, c) gradient magnitude-dependant shading + regular shadowing, d) gradient magnitude-dependant shading and shadowing (proposed method).

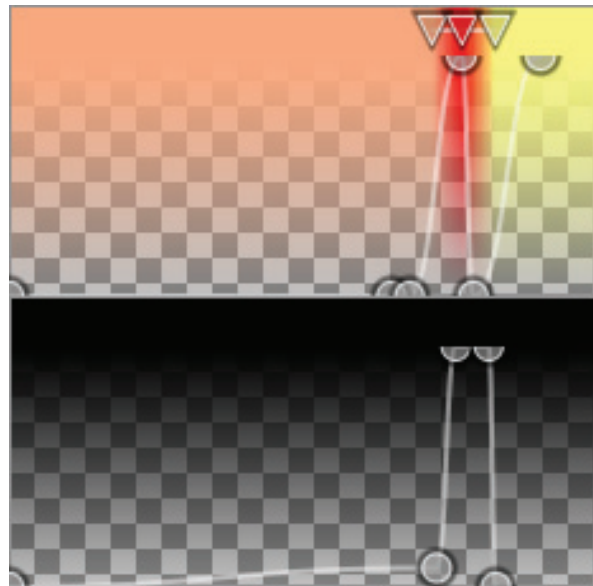


Figure 7: Opacity transfer function and corresponding shadow transfer function. Results, shown in Figure 10 were obtained with these transfer functions.

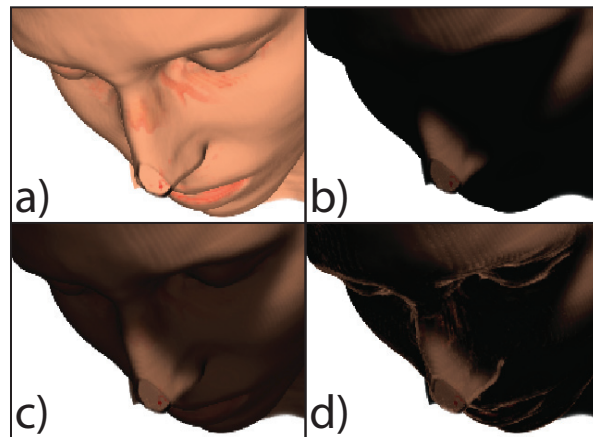


Figure 8: Human head dataset (opaque): a) no shadowing, b) regular shadowing, c) 80% shadowing, d) contour-preserving shadowing.

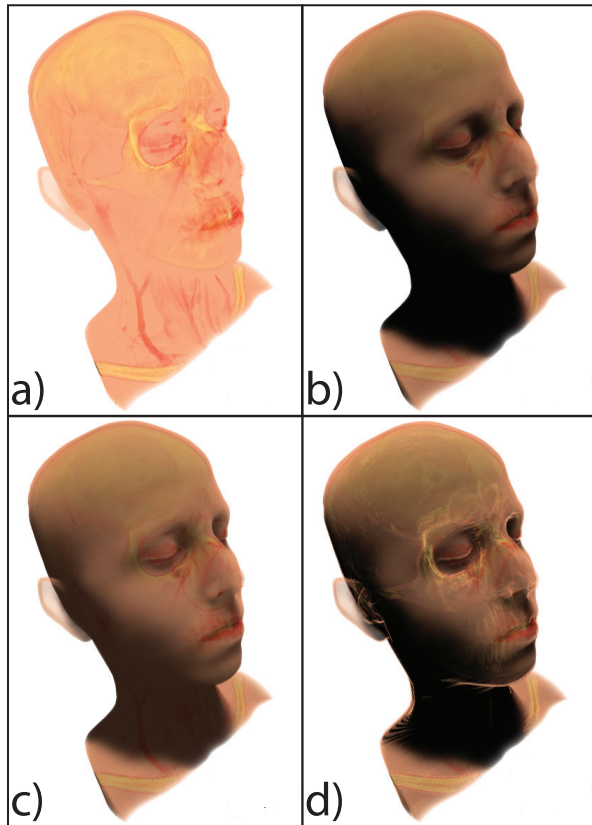


Figure 9: Human head dataset (translucent): a) no shadowing, b) regular shadowing, c) 80% shadowing, d) contour-preserving shadowing.

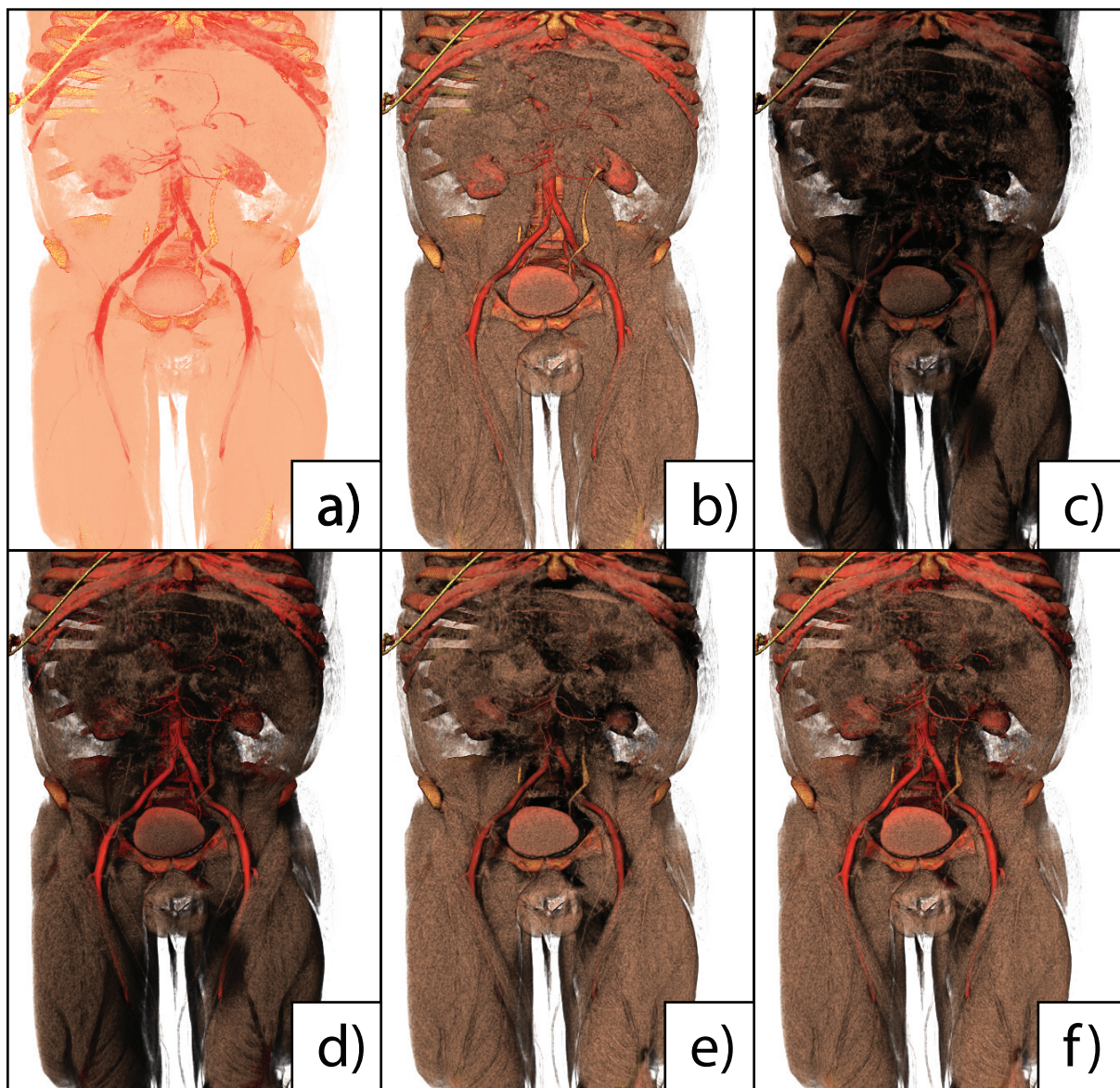


Figure 10: Human body dataset: a) no shading, b) Phong shading, c) shading + regular shadowing, d) shading + shadow receiver inconsistency, e) shading + shadow caster inconsistency, f) shading + shadow receiver and caster inconsistency.